

# Possible effects of pair echoes on gamma-ray burst afterglow emission

Kohta Murase,<sup>1\*</sup> Bing Zhang,<sup>2</sup> Keitaro Takahashi<sup>1</sup> and Shigehiro Nagataki<sup>1</sup>

<sup>1</sup>*Yukawa Institute for Theoretical Physics, Kyoto University, Sakyo-ku, Kyoto 606-8502, Japan*

<sup>2</sup>*Department of Physics and Astronomy, University of Nevada at Las Vegas, Las Vegas, NV 89154, USA*

Accepted 2009 February 24. Received 2009 February 23; in original form 2008 November 30

## ABSTRACT

High-energy emission from gamma-ray bursts (GRBs) is widely expected but had been sparsely observed until recently when the *Fermi* satellite was launched. If  $> \text{TeV}$  gamma-rays are produced in GRBs and can escape from the emission region, they are attenuated by the cosmic infrared background photons, leading to regeneration of  $\sim \text{GeV} - \text{TeV}$  secondary photons via inverse-Compton scattering. This secondary emission can last for a longer time than the duration of GRBs, and it is called a pair echo. We investigate how this pair echo emission affects spectra and light curves of high-energy afterglows, considering not only prompt emission but also afterglow as the primary emission. Detection of pair echoes is possible as long as the intergalactic magnetic field (IGMF) in voids is weak. We find (1) that the pair echo from the primary afterglow emission can affect the observed high-energy emission in the afterglow phase after the jet break and (2) that the pair echo from the primary prompt emission can also be relevant, but only when significant energy is emitted in the TeV range, typically  $\mathcal{E}_{\gamma, > 0.1 \text{ TeV}} > Y(1 + Y)^{-1} \epsilon_e \mathcal{E}_k$ . Even non-detections of the pair echoes could place interesting constraints on the strength of IGMF. The more favourable targets to detect pair echoes may be the ‘naked’ GRBs without conventional afterglow emission, although energetic naked GRBs would be rare. If the IGMF is weak enough, it is predicted that the GeV emission extends to  $> 30 - 300$  s.

**Key words:** magnetic fields – radiation mechanisms: non-thermal – gamma-rays: bursts.

## 1 INTRODUCTION

High-energy emission from gamma-ray bursts (GRBs) has been expected, and various theoretical possibilities have been discussed by numerous authors (see e.g. Fan & Piran 2008, and references therein). In fact, EGRET detected several GRBs with GeV emission (e.g. Hurley et al. 1994). Recently, the *Fermi* satellite was launched, and the onboard Large Area Telescope (LAT) is widely expected to detect high-energy ( $> \text{GeV}$ ) emission from a fraction of GRBs. In addition, other space- and ground-based gamma-ray observatories, such as AGILE, MAGIC, VERITAS and High Energy Stereoscopic System Observatory (HESS), also regard GRBs as one of the main scientific targets. Theoretically, there are the two main classes as high-energy emission mechanisms, i.e. leptonic and hadronic mechanisms. The leptonic mechanisms include synchrotron self-Compton (SSC) emission and external inverse-Compton emission, which are the most discussed scenarios for both the prompt and the afterglow emission components. High-energy SSC emission is produced by relativistic electrons that radiate seed synchrotron photons (e.g. Sari & Esin 2001; Zhang & Mészáros 2001; Guetta & Granot 2003). In addition, there are various possibil-

ities for external inverse-Compton emission. For example, prompt gamma-ray photons or the X-ray flare photons may act as seed photons for the relativistic electrons accelerated during the afterglow phase in the external shocks (e.g. Beloborodov 2005; Wang, Li & Mészáros 2006). The hadronic mechanisms include synchrotron radiation of high-energy baryons, synchrotron radiation of the secondary leptons generated in photohadronic interactions, as well as the photons directly produced from  $\pi^0$  decays. In order to see the baryon synchrotron radiation, sufficiently strong magnetic fields are typically required (e.g. Gupta & Zhang 2007; Murase et al. 2008a). Otherwise, photohadronic components would dominate over the baryon synchrotron component as long as the photon density is high enough. Hadronic gamma-rays can be observed only when the non-thermal baryon loading is large enough (e.g. Murase & Nagataki 2006; Asano & Inoue 2007). So far, both emission mechanisms have been widely considered in the standard scenario (see reviews e.g. Mészáros 2006; Zhang 2007), i.e. the internal shock model for the prompt emission and the external shock model for the afterglow emission, respectively.

Both mechanisms can, in principle, produce  $> 1 \text{ TeV}$  photons, although high-energy photons may not escape from the source due to two-photon pair production, especially during the prompt emission phase (Lithwick & Sari 2001; Granot, Cohen-Tanugi & do Couto e Silva 2008; Gupta & Zhang 2008; Murase & Ioka 2008). Even if

\*E-mail: kmurase@yukawa.kyoto-u.ac.jp

such super-TeV photons can escape from the source, they still suffer from pair creation due to the interaction with the cosmic infrared background (CIB) or the cosmic microwave background (CMB). In particular, the direct detection of TeV photons would be difficult for GRBs with redshift  $z > 1$ . On the other hand, the electron–positron pairs resulting from the pair creation are still energetic, so that they up-scatter numerous CMB photons via the inverse-Compton process. Such secondary photons are able to reach the observer in a longer duration than the duration of primary emission, and a significant fraction of them may be observed with a time delay due to several effects, such as magnetic deflection and angular spreading. Therefore, this emission is called ‘pair echo’ emission, with a typical energy in the range of  $\sim(1\text{--}100)$  GeV. This pair echo emission is not only indirect evidence of the intrinsic TeV emission but also a clue to probe the weak intergalactic magnetic field (IGMF) of  $B_{\text{IG}} < 10^{-16}$  G (Plaga 1995).

Plaga’s method is hitherto the only one to probe very weak magnetic fields of  $B_{\text{IG}} < 10^{-16}$  G. Other methods utilizing the Faraday rotation or CMB are sensitive to magnetic fields of the order of  $B_{\text{IG}} \sim 1$  nG (Kronberg 1994). The presence of very weak IGMFs has been predicted by several mechanisms, such as inflation (e.g. Turner & Widrow 1988), reionization (e.g. Gnedin, Ferrara & Zweibel 2000) and density fluctuations (e.g. Takahashi et al. 2005; Ichiki et al. 2006). Observations of IGMFs in voids would give important information on the origin of the galactic magnetic fields (Widrow 2002), although they may be contaminated by astrophysical sources, such as galactic winds or quasar outflows (Furlanetto & Loeb 2001).

In this paper, we reinvestigate the observational effects of the possible pair echo emission of GRB high-energy emission in the afterglow phase. Three criteria should be satisfied to detect pair echo emission: (1) the object must emit  $\sim$ TeV gamma-rays leading to pair echoes; (2) the pair echo flux must be higher than the detector’s flux sensitivity and (3) the pair echo emission component must not be masked by other emission components. Concerning the point (1), TeV photons from GRBs can be emitted during both the prompt and the afterglow phases. Here, we consider both as the primary emission components for the echoes, by acknowledging that during the prompt phase strong TeV gamma-rays are expected only for a small fraction of GRBs due to the large  $\gamma\gamma$  optical depth, as has been studied by various authors (Dai & Lu 2002; Razzaque, Mészáros & Zhang 2004; Murase, Asano & Nagataki 2007; Takahashi et al. 2008). Concerning the point (2), we need to evaluate the pair echo flux quantitatively. This flux depends on the amount of the CIB photons, the IGMF strength and the source distance. As for the CIB, we use the acceptable CIB models given by Kneiske, Mannheim & Hartmann (2002) and Kneiske et al. (2004). In order to take into account the effects of the IGMF properly, we adopt the formulation developed by Ichiki, Inoue & Takahashi (2008), which enables us to calculate the time-dependent spectra better than the previous works (Dai et al. 2002; Dai & Lu 2002; Razzaque et al. 2004; Wang et al. 2004; Murase et al. 2007). In addition, we have also taken into account up-scatterings of the CIB photons as well as the CMB photons. This effect was neglected in the previous work for simplicity (Takahashi et al. 2008), but it can be also important (Murase et al. 2007). In this work, we focus on the detectability of the *Fermi* LAT, which is the most suitable one for our purpose, but also touch upon the capabilities of other ground-based TeV detectors, such as MAGIC and VERITAS. Concerning the point (3), we pay special attention to the high-energy afterglow emission, which is the main competitor of the pair echoes, and compare its strengths with respect to the echo components. Such a comparison was not done for previous researchers who studied the pair echo.

At present, a detailed comparison between the pair echoes and high-energy afterglows is highly uncertain, as both have never been clearly detected. Since various predictions of high-energy emission rely on many model assumptions, they should be tested by observations of *Fermi*, MAGIC, VERITAS and other detectors. Despite these uncertainties, we think it would be interesting and important to study effects of pair echoes that can affect high-energy emission, especially in the late phase (Dai & Lu 2002; Razzaque et al. 2004; Murase et al. 2007; Takahashi et al. 2008).

## 2 EMISSION CHARACTERISTICS

### 2.1 GRB primary emission

For a typical long-duration GRB, prompt gamma-ray emission is observed in a duration of  $\Delta T \sim (10\text{--}100)$  s. The typical isotropic energy is around  $\mathcal{E}_\gamma^{\text{iso}} \sim 10^{53}$  erg. The observed specific flux spectrum is well approximated by a broken power law,  $F_\gamma \propto (E_\gamma/E_\gamma^b)^{-\alpha+1}$  for  $E_\gamma < E_\gamma^b$  and  $F_\gamma \propto (E_\gamma/E_\gamma^b)^{-\beta+1}$  for  $E_\gamma^b < E_\gamma$ , where  $E_\gamma^b$  is the break energy which is typically  $\sim 300$  keV.  $\alpha$  and  $\beta$  are the low- and high-energy photon indices, respectively. In this work, we extrapolate this spectrum to higher energies and adopt  $F_\gamma \propto (E_\gamma/E_\gamma^b)^{-\beta+1}$  for  $0.1 \text{ TeV} < E_\gamma < E_\gamma^{\text{cut}}$ , where  $E_\gamma^{\text{cut}}$  is the intrinsic cut-off energy which is typically determined by the opacity of pair production. Whether TeV gamma-rays can escape from the source strongly depends on the Lorentz factor and on the emission radius. Only when these quantities are large, do we expect TeV gamma-rays escaping from the source, i.e.  $E_\gamma^{\text{cut}} > 1$  TeV. Note that although the SSC or possible hadronic mechanism leads to more complicated spectra (e.g. Guetta & Granot 2003; Asano & Inoue 2007; Gupta & Zhang 2007), this simplification is sufficient for calculating the pair echo (e.g. Murase et al. 2007). The pair echo is a kind of regenerated processes, which is composed of up-scattered CMB and CIB photons. The resulting pair echo spectrum sensitively depends on the intrinsic cut-off energy, while it is not so sensitive to source electron spectral indices of  $p < 3$  for a given  $E_\gamma^{\text{cut}}$  (Murase et al. 2007). When the intrinsic cut-off energy is low enough, the resulting spectrum basically reflects the seed CMB and CIB spectra,<sup>1</sup> which roughly leads to the spectral peak of  $\sim[(1+z)E_\gamma^{\text{cut}}/2m_e c^2]^2 k_B T'_{\text{CMB}}/(1+z)$ . Here,  $T'_{\text{CMB}} = 2.73(1+z)$  K is the local CMB temperature. On the other hand, when the intrinsic cut-off energy is high enough, high-energy secondary photons are reabsorbed, and the resulting spectrum has the cut-off due to CMB/CIB absorption. As the intrinsic cut-off energy is higher, the cascade effect becomes more and more significant, i.e. repeating the pair creation and inverse-Compton scattering is important. It affects the resulting spectrum, erasing the memory of the primary spectrum in the high energies. Rather, the radiation energy output above TeV is important for the pair echo flux, and we normalize the primary flux through the isotropic radiation energy above 0.1 TeV,  $\mathcal{E}_{\gamma, > 0.1 \text{ TeV}}$ .

The prompt emission is followed by the afterglow phase, during which the relativistic ejecta is decelerated by a circumburst medium. A pair of external shocks (forward and reverse) forms,

<sup>1</sup> If the spectrum of relativistic pairs is expressed by a power law with an index of  $s$ , the inverse-Compton spectrum is expected as  $F_\gamma \propto e^{-\frac{s-1}{2}}$  below the peak. However, the pair spectrum is strongly affected by the CIB field and is proportional to  $[1 - e^{-\tau_{\gamma\gamma}(E_\gamma, z)}]$ , where  $\tau_{\gamma\gamma}(E_\gamma, z)$  is the optical depth of photons with  $E_\gamma$  emitted at the redshift  $z$ . Since the pair echo spectrum is rather sensitive to the IGMF and the CIB spectrum, it is not easy to know a source electron spectral index  $p$ .

from which electrons (and possibly baryons) are accelerated and radiate afterglow photons. High-energy emission during this phase was predicted by many authors in both the reverse and forward shock models. (see Fan & Piran 2008, and references therein). TeV emission in the external shocks has a smaller optical depth for pair production, and hence can escape the source more easily. For the forward shock, the characteristic energies for the SSC emission are given by (e.g. Sari & Esin 2001; Zhang & Mészáros 2001; Guetta & Granot 2003)

$$E_{\text{SSC}}^m \simeq 2.3 \times 10^3 \text{ eV } g^4 \epsilon_{e,-1}^4 \epsilon_{B,-2}^{\frac{1}{2}} \mathcal{E}_{k,53}^{\frac{3}{4}} n_0^{-\frac{1}{4}} t_4^{-\frac{9}{4}} \quad (1)$$

$$E_{\text{SSC}}^c \simeq 2.2 \times 10^{10} \text{ eV } \epsilon_{B,-2}^{-\frac{7}{2}} \mathcal{E}_{k,53}^{-\frac{5}{4}} n_0^{-\frac{9}{4}} (1+Y)^{-4} t_4^{-\frac{1}{4}}, \quad (2)$$

where  $\epsilon_B$  and  $\epsilon_e$  are the fractions of the shock energy transferred to the downstream magnetic fields and non-thermal electrons, respectively.  $g = g(p)$  is a numerical factor, which is expressed as  $g(p) = (p-2)/(p-1)$  for  $p > 2$  and the typical value for  $p \sim 2$  is  $g \sim 0.1$ .  $\mathcal{E}_k$  is the isotropic kinetic energy of the ejecta,  $n$  is the circumburst medium density<sup>2</sup> and  $Y$  is the Compton parameter. For  $\epsilon_e > \epsilon_B$ , we roughly have<sup>3</sup>  $Y \sim \sqrt{\epsilon_e/\epsilon_B}$  (e.g. Sari & Esin 2001; Zhang & Mészáros 2001), and the high-energy emission spectrum is written as  $F_{\text{SSC}} \propto E_{\text{SSC}}^{1/3}$  for  $E_{\text{SSC}} < E_{\text{SSC}}^m$ ,  $F_{\text{SSC}} \propto E_{\text{SSC}}^{-(p-1)/2}$  for  $E_{\text{SSC}}^m < E_{\text{SSC}} < E_{\text{SSC}}^c$  and  $F_{\text{SSC}} \propto E_{\text{SSC}}^{-p/2}$  for  $E_{\text{SSC}}^c < E_{\text{SSC}} < E_{\text{SSC}}^{\text{cut}}$ , where  $p \sim 2-3$  is the spectral index of the accelerated electrons. Here,  $E_{\text{SSC}}^{\text{cut}}$  is the cut-off energy determined by either the pair-creation opacity or the Klein–Nishina limit (e.g. Zhang & Mészáros 2001). The energy flux at the SSC peak (for  $p \sim 2$ ) is evaluated as

$$E_{\text{SSC}}^c F_{\text{SSC}}^c \simeq 2.7 \times 10^{-8} \text{ GeV cm}^{-2} \text{ s}^{-1} \times Y(1+Y)^{-1} g_{-1} \epsilon_{e,-1} \mathcal{E}_{k,53} t_4^{-1} D_{28}^{-2}, \quad (3)$$

by which we can normalize the SSC spectrum. The above temporal behaviour is typically valid from the break time of  $t_b \sim 10^4$  s to the next break time of  $t_j \sim 10^5$  s during the so-called normal decay phase of X-ray afterglow. Afterglow light curves of some GRBs are steepened after  $t_j$ , which is often interpreted as a jet break when the Lorentz factor  $\Gamma$  becomes the inverse of the jet opening angle<sup>4</sup>  $1/\theta_j$  (Rhoads 1999; Sari, Piran & Halpern 1999). The temporal behaviour after the jet break  $t_j$  is expected as  $E_{\text{SSC}}^c \propto t^{-3}$ ,  $E_{\text{SSC}}^m \propto t^1$ ,  $E_{\text{SSC}}^{\text{cut}} \propto t^{-1/2}$  and  $F_{\text{SSC}}^c \propto t^{-2}$ .

The afterglow behaviour before  $t_b$  cannot be interpreted by the standard afterglow model. As observed by *Swift*, a good fraction of X-ray afterglow has a shallow decay phase lasting from  $t_a \sim 10^3$  s (at which the shallow decay emission becomes dominant in x rays) to  $t_b \sim 10^4$  s (see e.g. Nousek et al. 2006; O’Brien et al. 2006), which has a decay slope of  $\propto t^{-(0-0.8)}$ . Several models have been proposed for explaining this phase (see e.g. Eichler & Granot 2006; Zhang et al. 2006; Genet, Daigne & Mochkovitch 2007; Ghisellini et al. 2007; Panaitescu 2007; Uhm & Beloborodov 2007; Yamazaki 2009), and one of the mostly discussed interpretations is continuous energy injection into the forward shock. Here, we consider the modified forward shock model with the energy injection of the form  $\mathcal{E}_k \propto t^{1-q}$ , where  $q$  parametrizes the energy injection and  $q = 1$  corresponds to the case of no energy injection. Such modified

forward shock models are supported by the lack of spectral evolution across  $t_b$  and the compliance of the ‘closure relations’ in the normal decay phase after  $t_b$  (Liang, Zhang & Zhang 2007a). During this phase, the temporal behaviour of various parameters is  $E_{\text{SSC}}^c \propto t^{-3/2-3q/4}$ ,  $E_{\text{SSC}}^m \propto t^{-3/2+5q/4}$ ,  $E_{\text{SSC}}^{\text{cut}} \propto t^{-q/4}$  and  $F_{\text{SSC}}^c \propto t^{-q}$  (Fan et al. 2008). We have calculated the high-energy light curves of the SSC emission during this phase. Similar calculations were performed by e.g. Gou & Mészáros (2007), Wei & Fan (2007) and Fan & Piran (2008).

## 2.2 Pair echo emission

Pair echoes are the up-scattered CMB and CIB photons by the electron–positron pairs produced via the attenuation of the primary TeV photons by the CIB. For a given primary spectrum, the total fluence of the pair echo emission is determined by the  $\gamma\gamma$  optical depth of the CIB, and does not depend on the IGMF as long as the deflection angle is much smaller than the jet opening angle. Primary photons with energy  $E_\gamma$  are converted to pairs with the Lorentz factor  $\gamma_e \approx 10^6$  ( $E_\gamma/1 \text{ TeV}$ )  $(1+z)$  in the local cosmological rest frame, which then up-scatter CMB and CIB photons. CMB photons are boosted to energies  $\sim 2.82 k_B T'_{\text{CMB}} \gamma_e^2 / (1+z) \approx 0.63 (E_\gamma/1 \text{ TeV})^2 (1+z)^2 \text{ GeV}$ . To evaluate the pair echo flux, we must consider various time-scales involved in the process, such as the angular spreading time, and the delay time due to magnetic deflections (e.g. Dai & Lu 2002; Dai et al. 2002; Razzaque et al. 2004). These can be estimated as follows (Takahashi et al. 2008; Murase et al. 2008b).

The angular spreading time is  $\Delta t_{\text{ang}} \approx (1+z) (\lambda'_{\text{IC}} + \lambda'_{\gamma\gamma}) / 2 \gamma_e c$ , where  $\lambda'_{\gamma\gamma} \approx (0.26 \sigma_T n'_{\text{CIB}})^{-1} \approx 20 \text{ Mpc} (n'_{\text{CIB}}/0.1 \text{ cm}^{-3})^{-1}$  is the local  $\gamma\gamma$  mean free path in terms of the local CIB photon density  $n'_{\text{CIB}}$ , and  $\lambda'_{\text{IC}} = 3 m_e c^2 / (4 \sigma_T U'_{\text{CMB}} \gamma_e) \approx 690 \text{ kpc} (\gamma_e/10^6)^{-1} (1+z)^{-4}$  is the local IC cooling length in term of the local CMB energy density  $U'_{\text{CMB}}$ . At the energies of our interest,  $\lambda'_{\gamma\gamma} \gg \lambda'_{\text{IC}}$  so that  $\Delta t_{\text{ang}} \approx (1+z) \lambda'_{\gamma\gamma} / 2 \gamma_e c \approx 960 \text{ s} (\gamma_e/10^6)^{-2} (n'_{\text{CIB}}/0.1 \text{ cm}^{-3})^{-1} (1+z)$ . For sufficiently small deflections in weak IGMFs with the present-day amplitude  $B_{\text{IG}} = B'_{\text{IG}}(1+z)^{-2}$  and coherence length  $\lambda_{\text{coh}} = \lambda'_{\text{coh}}(1+z)$ , the magnetic deflection angle is  $\theta_B = \min[\lambda'_{\text{IC}}/r_L, (\lambda'_{\text{IC}} \lambda'_{\text{coh}})^{1/2}/r_L]$ , where  $r_L = \gamma_e m_e c^2 / e B'_{\text{IG}}$  is the Larmor radius of the electrons or positrons.<sup>5</sup> The delay time due to magnetic deflection is  $\Delta t_B \approx (1+z) (\lambda'_{\text{IC}} + \lambda'_{\gamma\gamma}) (\theta_B^2/2c)$ . For coherent magnetic fields with  $\lambda'_{\text{coh}} > \lambda'_{\text{IC}}$ , we have  $\Delta t_B \approx \max[6.1 \times 10^3 \text{ s} (\gamma_e/10^6)^{-5} (B_{\text{IG}}/10^{-20} \text{ G})^2 (1+z)^{-7}, 1.6 \times 10^5 \text{ s} (\gamma_e/10^6)^{-4} (n'_{\text{CIB}}/0.1 \text{ cm}^{-3})^{-1} (B_{\text{IG}}/10^{-20} \text{ G})^2 (1+z)^{-3}]$ . Note that the deflection angle due to successive IC scattering  $\theta_{\text{IC}} \approx \sqrt{N} k_B T'_{\text{CMB}} / m_e c^2$  is usually very small, where  $N \approx \lambda'_{\text{IC}} / l'_{\text{IC}} \sim 1000$  is the number of scatterings and  $l'_{\text{IC}}$  is the IC scattering mean free path. We have also assumed that both  $1/\gamma_e$  and  $\theta_B$  do not exceed  $\theta_j$ , otherwise a significant fraction of photons or pairs will be deflected out of the line of sight and the echo flux is greatly diminished.

In order to calculate the pair echo flux, we adopt the formalism developed by Ichiki et al. (2008), which enables us to calculate the time-dependent spectra in a more satisfactory manner, particularly at late times, accounting properly for the geometry of the pair echo process. In previous works, explicit descriptions of the time-dependent spectra were not possible without some ad hoc modifications (Ando 2004; Murase et al. 2007).

<sup>5</sup> There was a typo on the expression of  $\theta_B$  in Murase et al. 2008b. The ‘minimum’ is correct rather than the ‘maximum’. The calculations were performed properly.

<sup>2</sup> We focus on the uniform medium in this work.

<sup>3</sup>  $Y \sim \sqrt{\epsilon_e/\epsilon_B}$  is expected when only the first SSC component is important. In fact, the second SSC component is typically negligible due to the Klein–Nishina suppression in the optically thin synchrotron scenario.

<sup>4</sup> Note that the predicted achromaticity of this jet-like break is only verified for a fraction of GRBs (Liang et al. 2008).

### 3 EFFECTS OF PAIR ECHOES ON HIGH-ENERGY AFTERGLOW EMISSION

In this section, we present our results and compare the pair echo emission with the afterglow emission. The detectability by the *Fermi*/LAT detector and the ground-based MAGIC telescope is also discussed. One main uncertainty stems from the CIB models, which can affect not only the pair echo fluence but also the time-scales for angular spreading and magnetic deflection at all redshifts. Recent high-energy observations of TeV blazars point to a low-infrared (IR) CIB model, close to the lower limit from the galaxy count data (e.g. Albert et al. 2008) (but see e.g. Stecker & Scully 2009). Hence, we here adopt the low-IR CIB model presented by Kneiske et al. (2002, 2004). More detailed discussion on the effects of the CIB is found in Murase et al. (2007). As for the afterglow parameters in the forward shock model, we adopt  $\mathcal{E}_k = 10^{52-53}$  erg,  $\epsilon_e = 0.1$ ,  $\epsilon_B = 0.01$ ,  $n = 1\text{cm}^{-3}$  and  $p = 2.0 - 2.4$ . We also assume the energy injection index  $q = 0.5$  before  $t_b = 10^4$  s, and take the jet break time as  $t_j = 10^5$  s.

#### 3.1 Afterglow-induced pair echoes versus afterglows

In Figs 1 and 2, we show the resulting spectra and light curves of the afterglow-induced pair echo and the primary afterglow emission. We can see that the echo component is outshined by the afterglow component during the shallow and normal decay phases. This result is consistent with Ando (2004), who argued that observed emission is unaffected by the pair echo. The situation changes dramatically after the jet break. The pair echo emission lasts for a long time because of the IGMF deflection of the pairs, and it can dominate the afterglow after the jet break by as much as an order of magnitude. It can be observed only for nearby GRBs with  $z < 0.2$  for our afterglow parameters.

If a GRB is very nearby and energetic, we may detect many photons at  $\sim\text{GeV}$  energies and even observe TeV photons during the afterglow phase. In such a case, in principle, a non-detection of the high-energy pair echo would allow us to obtain the lower limit on the IGMF. This is because if  $B_{\text{IG}} = 0$  one would expect an excess of the echo flux  $F_{\text{sec}}$  over the primary flux  $F_{\text{pri}}$ . The non-detection of the echo emission can then be attributed to the effect of a finite

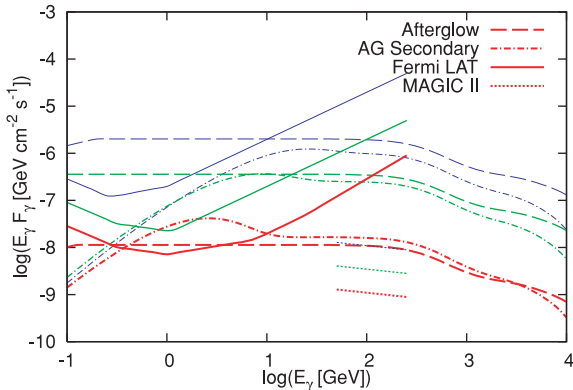


**Figure 1.** Primary and pair echo spectra for the canonical afterglow with  $\mathcal{E}_k = 10^{53}$  erg and  $p = 2.0$ , plotted at  $t = 10^{3.5}$  s (blue),  $10^{4.5}$  s (green) and  $10^{5.5}$  s (red), for the case of  $B_{\text{IG}} = 10^{-20}$  G,  $\lambda_{\text{coh}} = 1$  Mpc and  $z = 0.1$ . The *Fermi*/LAT and MAGIC II sensitivities (with the duty factor of 20 per cent) are also overlaid (Carmona et al. 2007). Note that the sensitivity curves in the sky survey mode are used for the long-time observations, although the possible continuous observations by LAT may improve the detectability by a factor of 3–5 (e.g. Gou & Mészáros 2007).

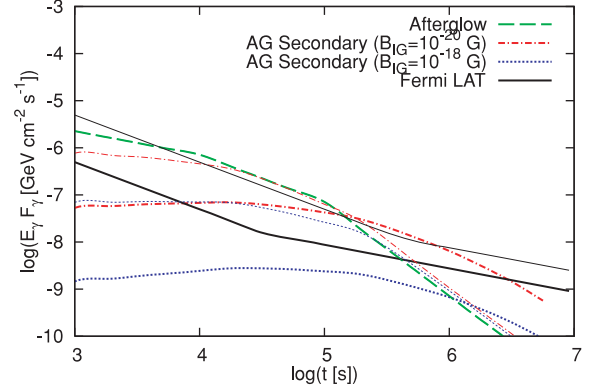


**Figure 2.** Primary and pair echo light curves for the canonical afterglow with  $\mathcal{E}_k = 10^{53}$  erg and  $p = 2.0$ , compared with the LAT sensitivity at 1 GeV (thick) and 10 GeV (thin), for the case of  $B_{\text{IG}} = 10^{-20}$  G with  $\lambda_{\text{coh}} = 1$  Mpc and  $B_{\text{IG}} = 10^{-18}$  G with  $\lambda_{\text{coh}} = 0.1$  kpc. The source redshift is  $z = 0.1$ .

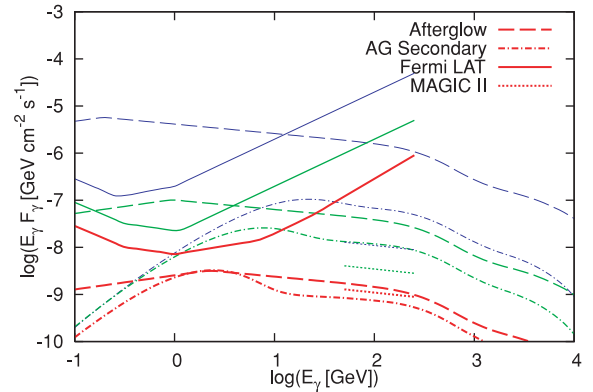


**Figure 3.** Same as Fig. 1, but for the canonical afterglow with  $\mathcal{E}_k = 10^{52}$  erg and  $p = 2.4$ .

IGMF, which deflects the secondary pairs to reduce the secondary echo flux to be  $F_{\text{sec}} < \max(F_{\text{pri}}, F_{\text{lim}})$ , where  $F_{\text{lim}}$  is the detector sensitivity (Murase et al. 2008b). The expected lower bound with our afterglow parameters ( $\mathcal{E}_k = 10^{53}$  erg and  $p = 2.0$ ) for a GRB with  $z = 0.1$  is estimated as

$$B_{\text{IG}} \min \left[ \lambda_{\text{coh}}^{1/2}, \lambda_{\text{IC}}^{1/2} \right] > 10^{-21} \text{ G Mpc}^{1/2}. \quad (4)$$

In general, the result depends on the source distance and on the afterglow parameters which should be determined from observational properties. In any case, the expected lower bounds are comparable to those derived for blazar flares (Murase et al. 2008b).

Similar to the case of blazar flares, one expects that whether the afterglow pair echo dominates over the primary emission depends on the high-energy afterglow spectrum. In Figs 3 and 4, we show the case of  $p = 2.4$ , corresponding to  $F_{\text{SSC}} \propto E_{\text{SSC}}^{-1.2}$ . Obviously, such steeper indices make it more difficult to see the afterglow-induced pair echo emission. This is just because steeper indices imply the smaller TeV flux compared to the GeV flux as for the afterglow emission. Hence, the electron spectral index is one of the uncertainties that are closely relevant to whether the afterglow-induced pair echoes are detectable. Also, it is clear that brighter afterglows are favourable for detections. Since the pair echo can be dominant over the afterglow itself only after the jet break, we need to observe a kind of energetic afterglows with  $Y(1+Y)^{-1} \epsilon_e \mathcal{E}_k > 10^{51.5}$  erg for  $z = 0.1$  (see Figs 1–4).

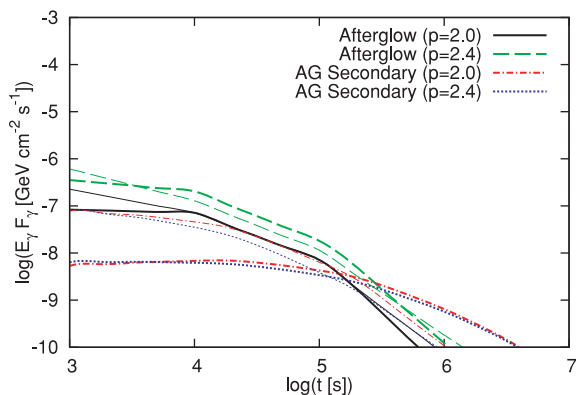


**Figure 4.** Primary and pair echo light curves for the canonical afterglow with  $\mathcal{E}_k = 10^{52}$  erg, for the cases of  $p = 2.0$  and  $2.4$ , respectively. Light curves at 1 GeV (thick) and 10 GeV (thin) are shown for the case of  $B_{\text{IG}} = 10^{-20}$  G with  $\lambda_{\text{coh}} = 1$  Mpc. The source redshift is  $z = 0.1$ .

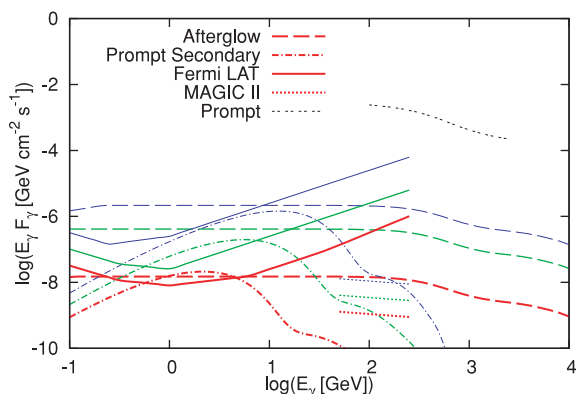


**Figure 5.** Spectra of the afterglow and the pair echo of the prompt emission, plotted at  $t = 10^{3.5}$  s (blue),  $10^{4.5}$  s (green) and  $10^{5.5}$  s (red), for the case of  $B_{\text{IG}} = 10^{-20}$  G with  $\lambda_{\text{coh}} = 1$  Mpc. The *Fermi*/LAT and MAGIC II sensitivities (with the duty factor of 20 per cent) also plotted for comparison. The prompt emission spectrum at  $t = 0$  s is shown, with  $\mathcal{E}_{\gamma, > 0.1 \text{ TeV}} = 10^{52}$  erg assumed. The canonical afterglow spectrum is also shown for the case of  $\mathcal{E}_k = 10^{53}$  erg and  $p = 2.0$ . The source redshift is  $z = 0.1$ .

### 3.2 Prompt-induced pair echoes versus afterglows

In Figs 5 and 6, we show the resulting spectra and light curves of the prompt-induced pair echo. The parameters for the primary prompt emission are taken as the following:  $\mathcal{E}_{\gamma, > 0.1 \text{ TeV}} = 10^{52}$  erg,  $\beta = 2.2$  and  $E_{\gamma}^{\text{cut}} = 10^{0.5}$  TeV. The duration in the local rest frame is set to  $\Delta T' = 25$  s. For comparison we also show the afterglow spectra/light curves. We note that the prompt-induced pair echo has been discussed by several authors before, but the comparison with the afterglow flux was never done previously. We find that the pair echo is observable only when GRBs are strong TeV emitters, i.e.  $\mathcal{E}_{\gamma, > 0.1 \text{ TeV}} > 10^{52}$  erg for our afterglow parameters [where  $Y(1+Y)^{-1}\epsilon_e \mathcal{E}_k > 10^{52}$  erg]. This is a strong requirement for the GRBs with canonical afterglows. For weak but non-zero IGMFs, the pair echo lasts for a longer time although its maximum flux is lower than the case of  $B_{\text{IG}} = 0$ . Then, the echo could still dominate over the afterglow at late times after the jet break, since its light curve is shallower than that of the afterglow.

In Figs 7 and 8, we show the more optimistic cases where brighter prompt emission and dimmer afterglow emission are assumed. In those cases, the observed behaviour of high-energy afterglows is quite different from the predicted one from the afterglow theory,

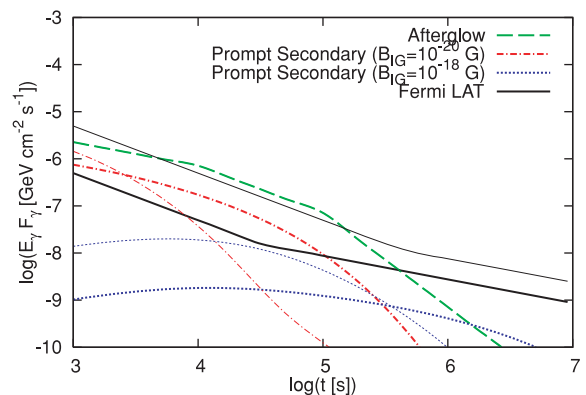


**Figure 6.** Light curves of the afterglow and the pair echo for the prompt emission compared with the LAT sensitivity at 1 GeV (thick) and 10 GeV (thin), for the case of  $B_{\text{IG}} = 10^{-20}$  and  $10^{-18}$  G with  $\lambda_{\text{coh}} = 0.1$  kpc. Here,  $\mathcal{E}_{\gamma, > 0.1 \text{ TeV}} = 10^{52}$  erg is assumed. The source redshift is  $z = 0.1$ .

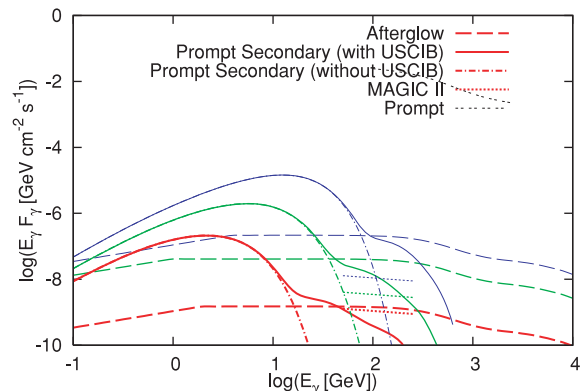


**Figure 7.** Spectra of the afterglow and the pair echo of the prompt emission, plotted at  $t = 10^{3.5}$  s (blue),  $10^{4.5}$  s (green) and  $10^{5.5}$  s (red), for the case of  $B_{\text{IG}} = 10^{-20}$  G with  $\lambda_{\text{coh}} = 1$  Mpc. The *Fermi*/LAT and MAGIC II sensitivities (with the duty factor of 20 per cent) also plotted for comparison. The prompt emission spectrum at  $t = 0$  s is shown, with  $\mathcal{E}_{\gamma, > 0.1 \text{ TeV}} = 10^{53}$  erg assumed. The canonical afterglow spectrum is also shown for the case of  $\mathcal{E}_k = 10^{52}$  erg and  $p = 2.0$ . The source redshift is  $z = 0.1$ . In order to demonstrate the effect of up-scattered cosmic infrared background (USCIB) photons (solid), curves without up-scattering of CIB photons are also shown (dot-dashed).

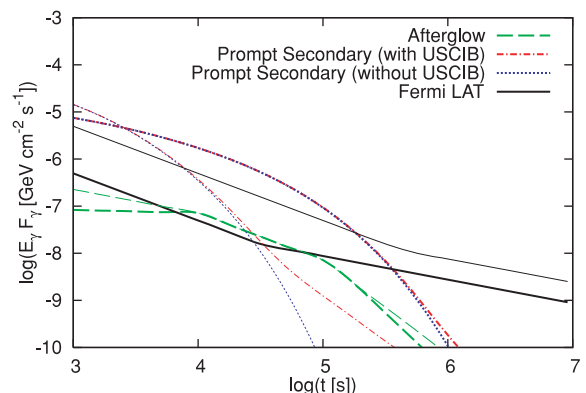


**Figure 8.** Light curves of the afterglow and the pair echo for the prompt emission compared with the LAT sensitivity at 1 GeV (thick) and 10 GeV (thin), for the case of  $B_{\text{IG}} = 10^{-20}$  and  $10^{-18}$  G with  $\lambda_{\text{coh}} = 0.1$  kpc. Here, the relevant parameters of the prompt emission and afterglow are the same as those used in Fig. 7. The source redshift is  $z = 0.1$ .

since the pair echo emission is dominant for a long time. A weak but non-zero IGMF with  $B_{\text{IG}} < 10^{-20}$  G can even make the pair halo outshine the shallow decay emission. In Figs 7 and 8, we also show the effect of up-scattered CIB photons. As is easily seen, their effect is important at high energies above 10–100 GeV, which can be crucial for detections through the MAGIC and VERITAS telescopes. Note that this effect becomes important when the intrinsic cut-off energy is not so high, as pointed out in Murase et al. (2007). Otherwise, the up-scattered CIB component is masked by the up-scattered CMB component. In fact, it is typically difficult to see the former for afterglow-induced pair echoes, where the pair echo spectrum at  $t$  is composed of the up-scattered CMB photons produced by the primary photons emitted at different times from the source.

Similar to what has been discussed in the previous section, one may obtain the lower bound on the IGMF for non-detection of the prompt-induced pair echo. However, the relative importance of the prompt-induced pair echo with respect to the afterglow emission is complicated, which strongly depends on the ratio of the prompt TeV emission energy and the electron energy in the afterglow ( $\epsilon_e \mathcal{E}_k$ ). In addition, the afterglow-induced pair echo would also contaminate the prompt-induced pair echo. Here, for a conservative estimate, let us consider the epochs of  $t < t_j$ . Assuming that TeV emission is detected, a non-detection of the pair echo would lead to

$$B_{\text{IG}} \min \left[ \lambda_{\text{coh}}^{1/2}, \lambda_{\text{IC}}^{1/2} \right] > 10^{-19.5} \text{ G Mpc}^{1/2}, \quad (5)$$

for our prompt and afterglow parameters used in Fig. 7.

#### 4 PAIR ECHOES FROM ‘NAKED’ GRBS

As seen in the previous section (see Figs 5 and 6), afterglow emission may significantly mask a pair echo (for both long and short GRBs). Hence, of special interest are the GRBs whose intrinsic high-energy afterglow emission is weak and whose prompt TeV emission is strong. Since almost all the long GRBs accompany afterglows, the possible candidates of such bursts are likely to be a fraction of short GRBs that do not show conventional X-ray afterglows (only show a steep decay phase as the tail of prompt emission spectrum). In fact,  $\sim 1/3$  of short GRBs (e.g. GRB 050906, 051210, 070209, 070810B and 080121) are such ‘naked’ bursts maybe due to the low density of the circumburst medium (e.g. La Parola et al. 2006). Since these bursts are spectrally hard and less energetic (than their long brethren), they may have prompt emission extending to the TeV range (e.g. Gupta & Zhang 2007). These bursts could therefore be the best targets to detect the pair echoes or to use non-detections to constrain the IGMF.

In Figs 9 and 10, we show the resulting spectra and light curves of the prompt-induced pair echo from a nearby, rather energetic short GRB. The parameters for the primary prompt emission are taken as the following:  $\mathcal{E}_{\gamma, > 0.1 \text{ TeV}} = 10^{51.5}$  erg,  $\beta = 2.2$  and  $E_{\gamma}^{\text{cut}} = 10^{0.5}$  TeV. The duration is set to  $\Delta T' = 1$  s. For naked GRBs, we expect that the primary emission decays according to the curvature effect, which typically drops as  $F_{\text{pri}} \propto t^{-3}$ . For instance, when  $E_{\gamma} F_{\gamma} \sim 10^{-2}$  GeV cm $^{-2}$  s $^{-1}$  during the burst, we have  $E_{\gamma} F_{\gamma} < 10^{-8}$  GeV cm $^{-2}$  s $^{-1}$  at  $t > 100$  s. Hence, we omit the afterglow spectra/light curves in Figs 9 and 10. As is seen in Fig. 10, the IGMF of  $B_{\text{IG}} \lambda_{\text{coh}}^{1/2} \sim 10^{-22}$  G Mpc $^{1/2}$  leads to the detectable flux at  $t \sim 10^4$  s, which should be observed as extended high-energy emission from short GRBs. Note that, when  $B_{\text{IG}} \sim 0$  G, the pair echo duration is determined by the angular spreading time,  $300 \text{ s} (n'_{\text{CIB}}/0.1 \text{ cm}^{-3})^{-1}$ . Therefore, it may typically be difficult for pair echoes to explain GeV emission whose time-scale is shorter (e.g. GRB 081024B and

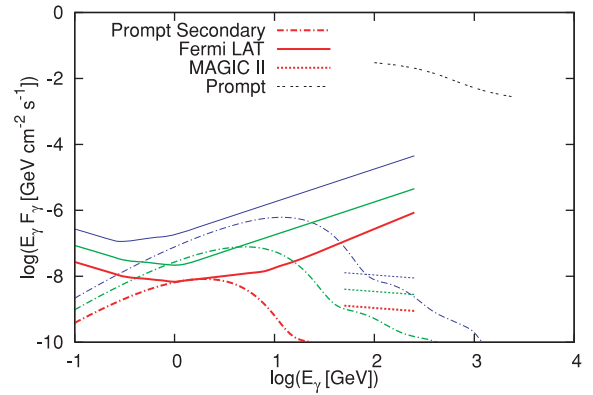


**Figure 9.** Spectra of the pair echo of the prompt emission from a naked short GRB, plotted at  $t = 10^{3.5}$  s (blue),  $10^{4.5}$  s (green) and  $10^{5.5}$  s (red), for the case of  $B_{\text{IG}} = 10^{-20}$  G with  $\lambda_{\text{coh}} = 1$  Mpc. The *Fermi/LAT* and *MAGIC II* sensitivities (with the duty factor of 20 per cent) are also plotted for comparison. The prompt emission spectrum at  $t = 0$  s is also shown, with  $\mathcal{E}_{\gamma, > 0.1 \text{ TeV}} = 10^{51.5}$  erg assumed. The source redshift is  $z = 0.1$ .

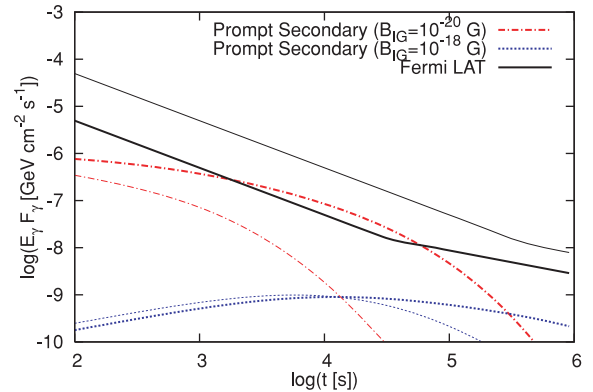


**Figure 10.** Light curves of the pair echo for the prompt emission from a naked short GRB compared with the *LAT* sensitivity at 1 GeV (thick) and 10 GeV (thin), for the case of  $B_{\text{IG}} = 10^{-20}$  and  $10^{-18}$  G with  $\lambda_{\text{coh}} = 0.1$  kpc. Here,  $\mathcal{E}_{\gamma, > 0.1 \text{ TeV}} = 10^{51.5}$  erg is assumed. The source redshift is  $z = 0.1$ .

see also discussions in Zou, Fan & Piran 2009), but they may also generate the high-energy extended emission.

For non-detections, one may obtain a constraint as

$$B_{\text{IG}} \min \left[ \lambda_{\text{coh}}^{1/2}, \lambda_{\text{IC}}^{1/2} \right] > 10^{-21.5} \text{ G Mpc}^{1/2}, \quad (6)$$

for our optimistic prompt parameters. We need to observe primary TeV emission for this purpose, but it is more difficult to make follow-up observations for short GRBs with *MAGIC* and *VERITAS*, compared to long GRBs. Note that significant and non-tentative TeV signals have not been observed so far for both the long and short GRBs (Abdo et al. 2007; Albert et al. 2007). This may be because a part of GRBs can be TeV emitters due to the small optical thickness for pair creation and TeV photons from distant sources are significantly attenuated by the CIB.

#### 5 SUMMARY AND DISCUSSION

In this paper, we have calculated the time-dependent spectra of the secondary pair echoes from the GRB prompt and afterglow TeV emission components that are attenuated by the CIB, applying a recently developed formalism to properly describe the temporal evolution of the pair echoes. We have compared the flux of the pair

echoes to that of the afterglow, taking into account up-scattering of the CIB photons. In particular, we have demonstrated (1) that afterglow-induced pair echoes can be important after the jet break for long GRBs with a canonical afterglow and (2) that prompt-induced pair echoes may also outshine the afterglow emission, if the prompt TeV emission is intense, typically with  $\mathcal{E}_{\gamma, > 0.1 \text{ TeV}} > Y(1+Y)^{-1}\epsilon_c\mathcal{E}_k$ .

Weak but non-zero IGMFs can be crucial for detectability, since they make the duration of the pair echo emission much longer than the time-scale of primary emission (see Figs 2, 4, 6 and 8). Although the detectability itself also depends on both the spectral evolution of the primary emission and detector sensitivities, such non-zero IGMFs can make it easier to detect secondary photons at late times when the pair echo emission remains shallow as compared to the afterglow emission. Concerning with the detection of pair echo signals, ‘naked’ (short) GRBs without a significant afterglow emission could be more promising. The pair echo should be observed as extended emission with the time-scale of  $t > 30\text{--}300$  s. The observational prospects of such pair echoes are quite interesting for the recently launched *Fermi*. Successful detections may be possible for nearby, bright events, and would open a new window to study the poorly unknown IGMF. Even in the case of non-detections, lower limits on the IGMF of  $B_{\text{IG}}\text{min}[\lambda_{\text{coh}}^{1/2}, \lambda_{\text{IC}}^{1/2}] \sim 10^{-20}\text{--}10^{-21}$  G Mpc<sup>1/2</sup> may be obtained.

The main caveat in hunting afterglow-induced pair echoes and pair echoes from short GRBs is that nearby bright GRBs do not seem frequent. Although there is large uncertainty on the nearby burst rate, the rate of bursts occurring within  $z \sim 0.3$  is estimated as  $\sim$  a few events per year (e.g. Guetta, Piran & Waxman 2005; Guetta & Piran 2006; Liang et al. 2007b). The actual detection rate also depends on several factors such as the detector sensitivity and field of view (e.g.  $\sim 2.4$  sr for the *Fermi*/LAT detector), so that only a fraction of them would be detected. If all the bursts are ideal TeV emitters, we can expect pair echoes for these bursts in the near future. However, it is unlikely that all the bursts are bright TeV emitters (and it seems more plausible for prompt emission due to significant attenuation by the pair creation). Although it is currently impossible to predict how many bursts can be bright TeV emitters in both the prompt and afterglow phases, the expected detection rate for  $z < 0.3$  bursts would be ‘at most’  $\sim 1\text{--}2$  events per year. There may be further complications about nearby GRBs. Some of the nearby long bursts detected so far seem somewhat dimmer than classical GRBs occurring at  $z > 1$ , but their local rate may be higher than the estimated local rate of classical GRBs (e.g. Guetta & Della Valle 2007; Liang et al. 2007b). Hence, we may have more nearby bursts that can be detected in the keV–MeV band by detectors with better sensitivities (e.g. *EXIST*). But, since the typical luminosity of such low-luminosity bursts seems small, it is not so easy to see pair echoes from them. In addition, energetic short GRBs assumed in Figs 9 and 10 would also be rare, whose radiation energy is larger than the typical one ( $\mathcal{E}_{\gamma}^{\text{iso}} \sim 10^{50\text{--}51}$  erg). Nevertheless, possible detections of pair echoes would bring us a big impact in understanding GRB physics and IGMF, even though the bright TeV GRBs that can lead to such detections are rare. The current on-orbit *Fermi* satellite is suitable for such a purpose. MAGIC and VERITAS can also provide valuable data via follow-up observations, since the pair echo emission can last for a long duration of time. In the near future, some constraints on the models may be achieved even for non-detections.

We must also be beware of the uncertainties in the intrinsic primary spectra since the pair echo flux depends on the amount of TeV photons. As for afterglow emission, we only consider the conven-

tional forward shock model with energy injection. Although other parameter sets or other models such as the varying  $\epsilon_c$  model can be considered, we expect that the qualitative features of the pair echoes themselves will not be changed significantly, as long as the light curve of high-energy emission is similar to that of X-rays and the amount of TeV photons is not too different from that invoked in our case. As for the prompt emission, possible uncertainties may come from the intrinsic emission properties such as  $E_{\gamma}^{\text{cut}}$ , as discussed in Murase et al. (2007).

The contamination by other high-energy emission components might complicate the picture further. There are many possibilities of high-energy gamma-ray emission during the afterglow phase (see e.g. Zhang 2007; Fan & Piran 2008, and references therein). For example, high-energy emissions associated with X-ray flares are expected at  $\sim$ GeV energies. GeV photons can be produced by both the leptonic mechanisms (e.g. Wang, Li & Mészáros 2006; Wei, Yan & Fan 2006; Yu & Dai 2008) and the hadronic mechanisms (Murase & Nagataki 2006). In addition, the reverse shock electrons can also provide high-energy photons during the early afterglow phase. None the less, it is, in principle, possible to distinguish the pair echo emission from other possibilities, given an ideal broadband (optical, X-ray, MeV and GeV) observational campaign.

## ACKNOWLEDGMENTS

KM and KT are supported by a Grant-in-Aid for the JSPS fellowship. BZ acknowledges NASA NNG05GB67G, NNX08AN24G and NNX08AE57A for support. SN is supported in part by Grants-in-Aid for Scientific Research from the Ministry of E.C.S.S.T. (MEXT) of Japan, nos. 19104006, 19740139 and 19047004. The numerical calculations were carried out on the Altix3700 BX2 at the YITP in the Kyoto University.

## REFERENCES

- Abdo A.-A. et al., 2007, *ApJ*, 666, 361
- Albert J. et al., 2007, *ApJ*, 667, 358
- Albert J. et al., 2008, *Sci*, 320, 1752
- Ando S., 2004, *MNRAS*, 354, 414
- Asano K., Inoue S., 2007, *ApJ*, 671, 645
- Beloborodov A.-M., 2005, *ApJ*, 618, L13
- Carmona E. et al., 2007, preprint (arXiv:0709.2959)
- Dai Z.-G., Lu T., 2002, *ApJ*, 580, 1013
- Dai Z.-G., Zhang B., Gou L.-J., Meszaros P., Waxman E., 2002, *ApJ*, 580, L7
- Eichler D., Granot J., 2006, *ApJ*, 641, L5
- Fan Y.-Z., Piran T., 2008, *Front. Phys. China*, 3, 306
- Fan Y.-Z., Piran T., Narayan R., Wei D.-M., 2008, *MNRAS*, 384, 1483
- Furlanetto S.-R., Loeb A., 2001, *ApJ*, 556, 619
- Genet F., Daigne F., Mochkovitch R., 2007, *MNRAS*, 381, 732
- Ghisellini G., Ghirlanda G., Nava L., Firmani L., 2007, *ApJ*, 658, L75
- Gnedin N.-Y., Ferrara A., Zweibel E.-G., 2000, *ApJ*, 539, 505
- Gou L.-J., Mészáros P., 2007, *ApJ*, 668, 392
- Granot J., Cohen-Tanugi J., do Couto e Silva E., 2008, *ApJ*, 677, 92
- Guetta D., Della Valle M., 2007, *ApJ*, 657, L73
- Guetta D., Granot J., 2003, *ApJ*, 585, 885
- Guetta D., Piran T., 2006, *A&A*, 453, 823
- Guetta D., Piran T., Waxman E., 2005, *ApJ*, 619, 412
- Gupta N., Zhang B., 2007, *MNRAS*, 380, 78
- Gupta N., Zhang B., 2008, *MNRAS*, 384, L11
- Hurley K. et al., 1994, *Nat*, 372, 652
- Ichiki K., Takahashi K., Ohno H., Hanayama H., Sugiyama N., 2006, *Sci*, 311, 827
- Ichiki K., Inoue S., Takahashi K., 2008, *ApJ*, 682, 127

- Kneiske T.-M., Mannheim K., Hartmann D.-H., 2002, *A&A*, 386, 1  
 Kneiske T.-M., Bretz T., Mannheim K., Hartmann D.-H., 2004, *A&A*, 413, 807  
 Kronberg P.-P., 1994, *Rep. Prog. Phys.*, 57, 325  
 La Parola V. et al., 2006, *A&A*, 454, 753  
 Liang E.-W., Zhang B.-B., Zhang B., 2007a, *ApJ*, 670, 565  
 Liang E.-W., Zhang B., Virgili F., Dai Z.-G., 2007b, *ApJ*, 662, 1111  
 Liang E.-W., Liang E.-W., Racusin J.-L., Zhang B., Zhang B.-B., Burrows D.-N., 2008, *ApJ*, 675, 528  
 Lithwick Y., Sari R., 2001, *ApJ*, 555, 540  
 Mészáros P., 2006, *Rep. Prog. Phys.*, 69, 2259  
 Murase K., Ioka K., 2008, *ApJ*, 676, 1123  
 Murase K., Nagataki S., 2006, *Phys. Rev. Lett.*, 97, 051101  
 Murase K., Asano K., Nagataki S., 2007, *ApJ*, 671, 1886  
 Murase K., Ioka K., Nagataki S., Nakamura T., 2008a, *Phys. Rev. D*, 78, 023005  
 Murase K., Takahashi K., Inoue S., Ichiki K., Nagataki S., 2008b, *ApJ*, 686, L67  
 Nousek J.-A. et al., 2006, *ApJ*, 642, 389  
 O'Brien P.-T. et al., 2006, *ApJ*, 647, 1213  
 Panaitescu A., 2007, *ApJ*, 379, 331  
 Plaga R., 1995, *Nat*, 374, 30  
 Razzaque S., Mészáros P., Zhang B., 2004, *ApJ*, 613, 1072  
 Rhoads J. E., 1999, *ApJ*, 525, 737  
 Sari R., Esin A.-A., 2001, *ApJ*, 548, 787  
 Sari R., Piran T., Halpern J., 1999, *ApJ*, 519, L17  
 Stecker F.-W., Scully S.-T., 2009, *ApJ*, 691, L91  
 Takahashi K., Ichiki K., Ohno H., Hanayama H., 2005, *Phys. Rev. Lett.*, 95, 121301  
 Takahashi K., Murase K., Ichiki K., Inoue S., Nagataki S., 2008, *ApJ*, 687, L5  
 Turner M.-S., Widrow L.-M., 1988, *Phys. Rev. D*, 37, 2743  
 Uhm Z.-L., Beloborodov A.-M., 2007, 665, L93  
 Wang X.-Y., Cheng K.-S., Dai Z.-G., Lu T., 2004, *ApJ*, 604, 306  
 Wang X.-Y., Li Z., Mészáros P., 2006, *ApJ*, 641, L89  
 Wei, D.-M., Fan, Y.-Z. 2007, *Chin. J. Astron. Astrophys.*, 7, 509  
 Wei D.-M., Yan T., Fan Y.-Z., 2006, *ApJ*, 636, L69  
 Widrow L.-M., 2002, *Rev. Mod. Phys.*, 74, 775  
 Yamazaki R., 2009, *ApJ*, 690, L118  
 Yu Y.-W., Dai Z.-G., 2008, *ApJ*, 692, 133  
 Zhang B., 2007, *Chin. J. Astron. Astrophys.*, 7, 1  
 Zhang B., Mészáros P., 2001, *ApJ*, 559, 110  
 Zhang B., Fan Y.-Z., Dyks J., Kobayashi S., Mészáros P., Burrows D.-N., Nousek J. A., Gehrels N., 2006, *ApJ*, 642, 354  
 Zou Y.-C., Fan Y.-Z., Piran T., 2009, *MNRAS*, in press (doi:10.1111/j.1365-2966.2009.14779.x) (arXiv:0811.2997)

This paper has been typeset from a  $\text{\TeX}/\text{\LaTeX}$  file prepared by the author.